

Identification of Piperidine-3-carboxamide Derivatives Inducing Senescence-like Phenotype with Antimelanoma Activities

Sangmi Oh, Do Yoon Kwon, Inhee Choi, Young Mi Kim, Ji Young Lee, Jiyoung Ryu, Hangeol Jeong, Myung Jin Kim,* and Rita Song*

Cite This: *ACS Med. Chem. Lett.* 2021, 12, 563–571

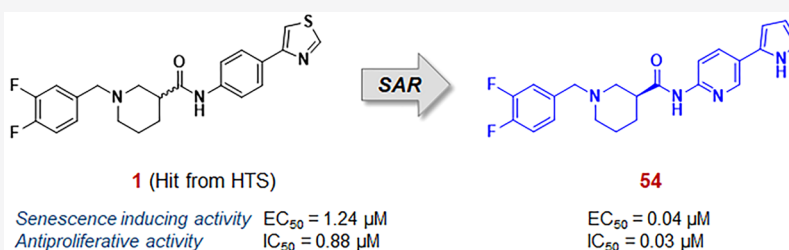
Read Online

ACCESS |

Metrics & More

Article Recommendations

Supporting Information



ABSTRACT: This study evaluated the potential use of senescence-inducing small molecules in the treatment of melanoma. We screened commercially available small-molecule libraries with high-throughput screening and high-content screening image-based technology. Our findings showed an initial hit with the embedded *N*-arylpiperidine-3-carboxamide scaffold-induced senescence-like phenotypic changes in human melanoma A375 cells without serious cytotoxicity against normal cells. A focused library containing diversely modified analogues were constructed and examined to evaluate the structure–activity relationship of *N*-arylpiperidine-3-carboxamide derivatives starting from hit **1**. This work identified a novel compound with remarkable antiproliferative activity *in vitro* and demonstrated the key structural moieties within.

KEYWORDS: high-throughput screening, high-content screening, senescence, melanoma, piperidine-3-carboxamide, structure–activity relationship

Cellular senescence is a cessation of cell division involving complex signal transduction pathways within the cells.^{1–3}

Two types of cellular senescence have been described in the literature: replicative senescence and premature senescence. Replicative senescence has been observed in all metabolic active cells, manifested as a spontaneous growth rate decline by telomere shortening. Replicative senescence could be recovered by ectopic expression of telomerase holoenzyme (hTERT).^{4–6} Premature senescence can be induced by oncogenes, chemicals, or oxidative stress.^{7,8} Senescent cells are characterized by altered cell morphology, including enlarged cell size, flattened cell shape, a single large nucleus, and increased cytoplasmic granularity. They could be distinguished from quiescent cells by their altered metabolic and transcriptional activities.

Recently, senescence is emerging as a therapeutic target for various diseases.^{9,10} Prosenescent and antisenescent therapies, called senolytic, showed promising results in mouse models, and human clinical trials are currently in progress. Some of the most widely used senolytics are BCL-2 family inhibitors that target apoptotic resistance of senescent cells.^{11,12} Conversely, drugs that induce senescence (such as palbociclib and other CDK4/6 inhibitors) have shown significant benefits as anticancer agents.^{13–18} The induction of senescence can lead

to a terminal nonproliferation state in cancer cells and/or result in apoptosis. In addition, senescent cells could be eliminated by CD4+T cells and macrophages, leading to an apoptosis-like effect.^{19–21} The genes involved in senescence and detailed mechanisms in anticancer therapies remain to be fully elucidated, and many research groups have been focusing on the identification of target proteins in the senescence pathway or small molecules that can induce senescence through library screening.^{13–16}

Senescence-associated β -gal (SA- β -gal) activity of cells has been widely used as a senescence marker in the screening for the discovery of senescence inducers.^{14,16} However, it is difficult to be applied to the high-throughput assay format due to the use of bright-field microscopy. To efficiently conduct high-throughput screening (HTS) and high-content screening (HCS), a whole-cell-based approach was designed to select compounds by analyzing the unique phenotype of senescent

Received: October 26, 2020

Accepted: March 17, 2021

Published: March 22, 2021



cells with fluorescence dye.²² With this technology, we screened ~110,000 chemicals and selected compounds that induced a senescence-like phenotype in human melanoma A375 cells. With image-based HTS/HCS, we identified compound **1** (Figure 1) as one of the initial hits to induce

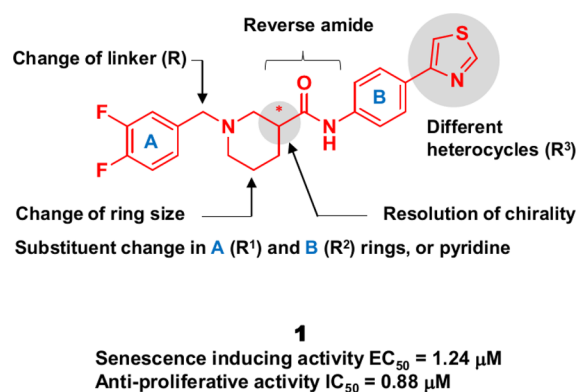


Figure 1. Hit compound **1** and its derivatization for SAR study.

senescence-like phenotypic changes in human melanoma A375 cells without serious cellular toxicity (Table SI-1). We here report the structure–activity relationship (SAR) study of *N*-arylpiperidine-3-carboxamide derivatives starting from **1**, which led to the identification of **54**, a novel compound with remarkable antimelanoma activity *in vitro*.

In search of compounds with improved antiproliferative activity as a senescence inducer, the initial hit **1** having the *N*-arylpiperidine-3-carboxamide moiety was chemically derivatized, as shown in Figure 1. General synthetic routes for *N*-arylpiperidine-3-carboxamide analogues were classified into three different ways, routes I–III, depending on the modification sites described in Schemes 1 and 2. Boc-protected *N*-bromophenyl heterocyclic carboxamides **4** were obtained by the EDC coupling reaction of 4-bromoaniline (**2**) and commercially available heterocyclic carboxylic acids (**3**). In the case of final products with a modified A ring or ring size of nitrogen-containing aliphatic cycle (**12–16**, **19–34**, **51**), they

were prepared by Suzuki coupling with **5**²³ followed by reductive amination with corresponding substituted benzaldehydes (**12–14**, **19–34**) in the presence of $\text{NaBH}(\text{OAc})_3$. Other derivatives with a modified linker part like carbonyl (**15**) and sulfone (**16**) were prepared through substitution reactions in the presence of base after Boc deprotection (route I in Scheme 1).

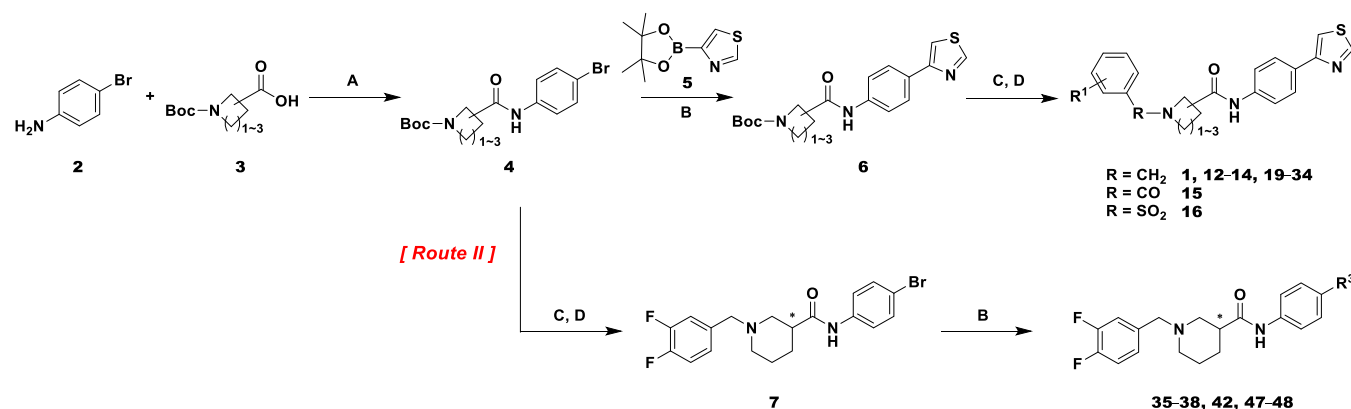
On the other hand, after Boc deprotection of intermediate **4**, reductive amination with 3,4-difluorobenzaldehyde and Suzuki coupling reaction with various boronic acid building blocks in sequence described in route II were applied for the synthesis of some derivatives having different heterocycles in the R^3 position (**35–38**, **42**, **47**, **48**).²⁴

The preparation of other analogues, modified B ring and/or R^3 position (**39–41**, **43–46**, **50–56**), were done starting from C–C bond formation between the B ring and R^3 (route III in Scheme 2). The key intermediates **10** were prepared by Suzuki coupling reaction with corresponding heterocyclic boronic acids except for **41** having a 2'-imidazolyl group. In this case, the condensation of imidazole with aryldiazonium ion *in situ* generated by 4-nitroaniline **9** in the presence of sodium nitrite, followed by nitro reduction for the synthesis of intermediate **10**.²⁵ Amide coupling reaction with Boc-nipecotic acid and then subsequent reductive amination led to the desired final compounds (Scheme 2). In addition, compound **17**, with a reverse amide between aminopiperidine and the B ring, was synthesized for the evaluation of amide linker via a Suzuki coupling reaction followed by amide coupling reaction (Scheme SI-5). The bicyclic benzothiazole **18** was generated by the same reaction described in Scheme 2 except with Suzuki coupling (Scheme SI-6). Detailed synthetic procedures including the synthesis of the most potent analogue **54** are described in Supporting Information. All final compounds newly synthesized were characterized by melting point, low resolution ESI mass, and ¹H NMR.

To assess anticancer activities of synthetic derivatives against melanoma cells, a phenomic assay was developed to measure cellular morphological changes such as enlarged cytoplasm containing a large nucleus and increased cytoplasmic granules along with counting the number of cells in a well. Doxorubicin,

Scheme 1^a

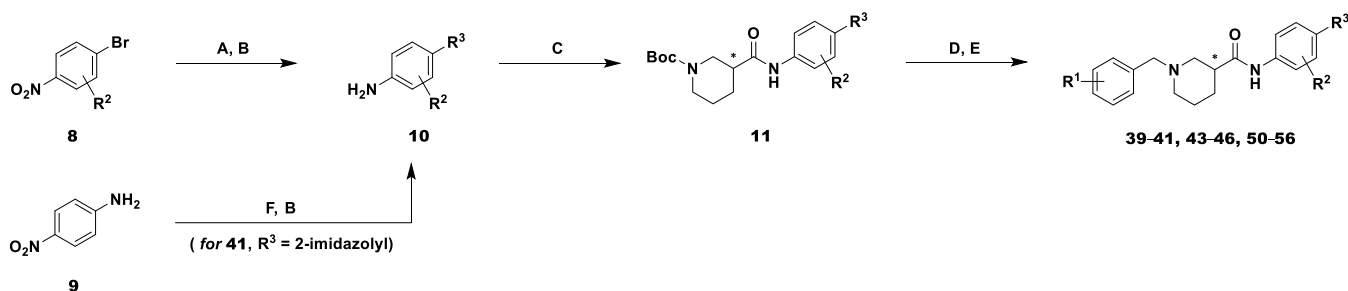
[Route I]



^aReagents and conditions: (A) EDC 1.2 equiv, HOBt 1.0 equiv, TEA 1.5 equiv, CH_2Cl_2 , RT, 12 h; (B) **5** or R^3 -boronic acid 1.2 equiv, $\text{Pd}(\text{PPh}_3)_4$ 0.05 equiv, Na_2CO_3 2.0 equiv, DME/ H_2O , 90 °C, 5 h; (C) 4 M HCl in dioxane, CH_2Cl_2 , RT, 2 h; (D) [$R = \text{CH}_2$] substituted benzaldehyde 1.2 equiv, $\text{NaBH}(\text{OAc})_3$ 2.0 equiv, AcOH (cat.), CH_2Cl_2 , RT, 12 h; [$R = \text{SO}_2$ or CO, $n = 1$] 3,4-difluorobenzesulfonyl chloride or 3,4-difluorobenzoyl chloride 1.2 equiv, TEA 2.0 equiv, CH_2Cl_2 , 0 °C, 3 h.

Scheme 2^a

[Route III]



^aReagents and conditions: (A) R³-boronic acid 1.2 equiv, Pd(PPh₃)₄ 0.05 equiv, Na₂CO₃ 2.0 equiv, DME/H₂O, 90 °C, 5 h; (B) 10% Pd/C, H₂ gas, MeOH, 0.5–2 h; (C) Boc-nipicotic acid 1.2 equiv, HATU 1.2 equiv, DIPEA 2.0 equiv, DMF, RT, 12 h; (D) TFA, CH₂Cl₂, RT, 1–3 h; (E) substituted benzaldehyde 1.2 equiv, NaBH(OAc)₃ 2.0 equiv, AcOH (cat.), CH₂Cl₂, RT, 12 h; (F) NaNO₂ 1.0 equiv, aq HCl and then imidazole 1.0 equiv, NaOAc, 0 °C to RT, 48 h.

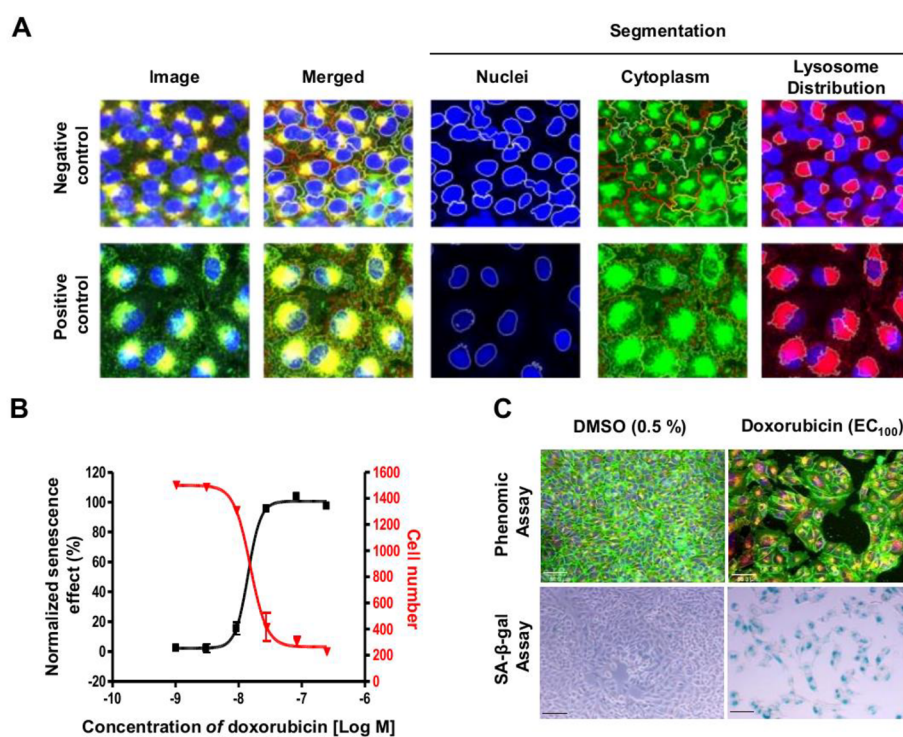


Figure 2. Assay validation with doxorubicin-treated cells. (A) Segmented images of negative control (0.5% DMSO) and positive control (37 nM doxorubicin in 0.5% DMSO) for data analysis. (B) Dose-dependent changes of doxorubicin-treated cells. Measurement of cell growth and senescence effect was analyzed by a customized algorithm. All experiments were duplicated. (C) Senescence effect of doxorubicin (37 nM in 0.5% DMSO) in phenomic assay and SA-β-gal assay. Human melanoma A375 cells were treated with or without doxorubicin (37 nM) for 3 days. In the phenomic assay, the cells were acquired images after staining with Hoechst 33342, LysoTracker Red DND-99, and CellMask (top panel). Under the same condition, cells were performed SA-β-gal (bottom panel). Scale bar is 50 μm.

a topoisomerase II inhibitor, was used to validate the assay (Figure 2) because it had been reported to induce DNA-damage-mediated senescence in human cells.^{26–28} After 3 days of compound treatment, human melanoma A375 cells were imaged and analyzed by customized software. Prior to analyses, the customized algorithm calibrated the segmentation procedure of images (Figure 2A). Morphological properties were captured and analyzed, including number of cells per well, cell size, nucleus size, granule size, the distance of each granule, cytoplasmic texture, volume of each organelle, etc. The EC₅₀ and IC₅₀ values were calculated from the dose–response curves based on cell number and ratio of senescent cells per well (Figure 2B). SA-β-gal assay, a traditional marker of

senescence, was also used to validate the senescence in doxorubicin-treated cells (Figure 2C). Under the same condition, doxorubicin-treated cells demonstrated highly increased SA-β-gal activity. *In vitro* antimelanoma activities of the synthetic compounds are summarized in Tables 1 and 2.

The hit compound **1** showed moderate senescence-inducing activity (EC₅₀ = 1.24 μM) and antiproliferative activity (IC₅₀ = 0.88 μM) in A375 human melanoma cell line (Figure 1 and Table 1). The piperidine-3-carboxamide moiety was important in both regioisomeric aspects and ring size because the regioisomer **12** with piperidine-4-carboxamide functionality was found to be inactive, and also the replacement of piperidine with smaller ones, pyrrolidine **13** or azetidine **14**,

Table 1. Senescence-inducing Activity (EC_{50}) and Antiproliferative Activity (IC_{50}) of *N*-Arylpiperidine-3-carboxamide Derivatives

Compound ^a	Chemical Structure	Activity (μ M)	
		EC_{50} ^b	IC_{50} ^c
1		1.24	0.88
12		19.0	>20
13		8.00	10.0
14		>20	>20
15		>20	>20
16		>20	>20
17		>20	>20
18		>20	>20
Doxorubicin		0.009	0.008

^aCompound 1 was an already known molecule. ^b EC_{50} means the effective concentration of a compound that induces senescence in a half population. ^c IC_{50} represents the concentration of a compound where the cell number is reduced by 50%.

displayed gradually decreasing activities (8.0 and >20 μ M, respectively). In addition to that, carbonyl (15) or sulfonyl groups (16) instead of a methylene linker were not effective to induce senescence. The reverse-amide analogue (17) of the original scaffold and bicyclic benzothiazole 18 also proved to be inactive.

In addition to evaluate the substituent effects of the A and B rings, and replacement effect of R with different heteroaryls, a series of compounds described in Table 2 were synthesized to determine the enantioselectivity toward antimelanoma activity. Notably, putative target molecules displayed a high level of enantioselectivity for *N*-arylpiperidine-3-carboxamide derivatives. *S*-Configuration 20 of the hit 1 showed an EC_{50} of 0.27 μ M, better than that of racemic mixture 1 and a 15-fold increase over that of *R*-configuration 19. This enantioselectivity also confirmed that *S*-configuration 50 had an EC_{50} of 0.14

μ M, much better than that of *R*-configuration 49 (19.9 μ M), while the EC_{50} of racemate 48 was 0.72 μ M.

In regard to substituent effects of R¹ in the A ring, the antiproliferative activity related to the senescence-like phenotype was strongly influenced by the presence of electronegative atoms, such as fluorine or oxygen, and their substitutional positions. Compounds without fluorine in C-2 and/or C-3, or regioisomers substituted in different positions of the A ring resulted in a significant loss of antimelanoma activities (21–26). Only 2,3,4-trifluoro-substituted 27 (EC_{50} = 1.26 μ M) showed potency similar to that of initial hit 1, and benzodioxole 34 (EC_{50} = 0.60 μ M), which was an oxygen-incorporated analogue at the position of C-2 and C-3, exhibited activity better than that of 1. Therefore, this finding indicated that the presence of hydrogen bonding acceptors at the C-2 and C-4 position might be essential for their antiproliferative activity against melanoma cancer cells. Other compounds including bulkier substituents in the A ring or pyridine instead of benzene were inactive (29–33).

To optimize R³ connected to the B ring, compounds 35–48 with various heterocycles were prepared and evaluated for their biological activities. Replacement of the original thiazole by six-membered aryl groups such as phenyl or pyridine (35–38) did not show an improvement of activity. However, five-membered heterocycles containing nitrogen or sulfur in the α -position were able to enhance antimelanoma activities (39, 42, 46, and 48). Even though all four derivatives showed a similar range of antiproliferative activities below 1.0 μ M as senescence inducers, we selected 2'-pyrrole as R³ for further modification because it has higher metabolic stability than the others (Table SI-2). Considering all of the structural factors detected in the SAR study, *S*-isomers 50 and 51 were prepared and found to have 10-fold increase in antimelanoma activities with senescence-like phenotype (EC_{50} = 0.14 and 0.16 μ M, respectively). To be able to search for proper modification of the B ring on the basis of 50, analogues 52–56 with different substituents on the B ring or with pyridine instead of benzene B ring were evaluated. A remarkable improvement in the biological activity was achieved when benzene was replaced with pyridine as the B ring, and 54 was found to be the most potent compound in the focused library with an EC_{50} of 40 nM, which was comparable to that of reference drug, doxorubicin (9 nM). Phase 1 metabolic stability studies of some synthetic analogues including hit 1 and 54 were performed for the future applications and confirmed that they were stable enough to test *in vivo* (see Table SI-2).

To check the activity of *N*-arylpiperidine-3-carboxamide and its derivatives on human melanoma A375 cells, the dose-dependent responses were examined via a newly developed phenomic assay. Compound 1 elicited phenomic changes and decreased total cell numbers (Figure 3A). Compared to hit 1, 54 was more potent to induce cell growth inhibition and a senescence-like phenotype (Figure 3B). To confirm the senescence-like morphological change by compound 54, we compared the morphological changes of 54-treated cells with doxorubicin-treated ones. Compound 54-treated cells showed a senescence-like phenotype which enlarged cell size and nucleus size with increasing cytoplasmic granularity, similar to doxorubicin-treated cells (Figure 3C).

A data set of 46 compounds in Tables 1 and 2 were used to build a pharmacophore model based on their senescence-inducing activity (EC_{50}). All of the structures were built on Maestro, a module of Schrödinger (Maestro). Low-energy 3D

Table 2. Senescence-inducing Activity (EC_{50}) and Antiproliferative Activity (IC_{50}) of *N*-Arylpiperidine-3-carboxamide Derivatives

Compound ^a	Chemical Structure				Activity (μ M)	
	Stereoisomer	R ¹	R ²	R ³	EC_{50} ^b	IC_{50} ^c
1	R+S	2,3-difluoro	H	4'-thiazolyl	1.24	0.88
19	R	2,3-difluoro	H	4'-thiazolyl	4.00	6.00
20	S	2,3-difluoro	H	4'-thiazolyl	0.27	0.19
21	R+S	H	H	4'-thiazolyl	>20	>20
22	R+S	1-fluoro	H	4'-thiazolyl	7.00	4.00
23	R+S	2-fluoro	H	4'-thiazolyl	5.00	2.45
24	R+S	3-fluoro	H	4'-thiazolyl	5.00	2.25
25	R+S	2,4-difluoro	H	4'-thiazolyl	1.50	1.36
26	R+S	1,2-difluoro	H	4'-thiazolyl	10.0	1.48
27	R+S	2,3,4-trifluoro	H	4'-thiazolyl	1.26	0.40
28	R+S	2,3-dichloro	H	4'-thiazolyl	3.00	1.73
29	R+S	2-methoxy	H	4'-thiazolyl	>20	>20
30	R+S	2-trifluoromethyl	H	4'-thiazolyl	>20	>20
31	R+S	2-trifluoromethoxy	H	4'-thiazolyl	>20	>20
32	R+S	2C \rightarrow 2N ^d	H	4'-thiazolyl	>20	>20
33	R+S	2-NHN=CH-3	H	4'-thiazolyl	>20	>20
34	R+S	2-OCH ₂ O-3	H	4'-thiazolyl	0.60	0.63
35	R+S	2,3-difluoro	H	phenyl	5.00	2.58
36	R+S	2,3-difluoro	H	4'-pyridyl	1.18	0.60
37	R+S	2,3-difluoro	H	3'-pyridyl	1.06	0.61
38	R+S	2,3-difluoro	H	2'-pyridyl	11.0	9.00
39	R+S	2,3-difluoro	H	2'-thiazolyl	0.80	0.24
40	R+S	2,3-difluoro	H	4'-imidazolyl	16.0	>20
41	R+S	2,3-difluoro	H	2'-imidazolyl	8.00	19.0
42	R+S	2,3-difluoro	H	5'-pyrazolyl	0.58	0.52
43	R+S	2,3-difluoro	H	3'-furanlyl	3.00	1.29
44	R+S	2,3-difluoro	H	2'-furanlyl	2.20	1.04
45	R+S	2,3-difluoro	H	3'-thiophenyl	1.93	0.95
46	R+S	2,3-difluoro	H	2'-thiophenyl	0.53	0.39
47	R+S	2,3-difluoro	H	3'-pyrrolyl	2.61	1.42
48	R+S	2,3-difluoro	H	2'-pyrrolyl	0.72	0.36
49	R	2,3-difluoro	H	2'-pyrrolyl	19.9	18.0
50	S	2,3-difluoro	H	2'-pyrrolyl	0.14	0.19
51	S	2-OCH ₂ O-3	H	2'-pyrrolyl	0.16	0.22
52	R+S	2,3-difluoro	1-methoxy	4'-thiazolyl	4.00	0.58
53	S	2,3-difluoro	1-fluoro	2'-pyrrolyl	0.10	0.13
54	S	2,3-difluoro	1C \rightarrow 1N ^d	2'-pyrrolyl	0.04	0.03
55	S	2,3-difluoro	2C \rightarrow 2N ^d	2'-pyrrolyl	4.00	3.01
56	S	2,3-difluoro	2-methyl	2'-pyrrolyl	3.00	0.73
Doxorubicin					0.009	0.008

^aCompounds 1, 21, 29, and 32 are already known molecules. ^b EC_{50} means the effective concentration of a compound that induces senescence in a half population. ^c IC_{50} represents the concentration of a compound where the cell number is reduced by 50%. ^dOne specific carbon in benzene was replaced by nitrogen with the formation of pyridine.

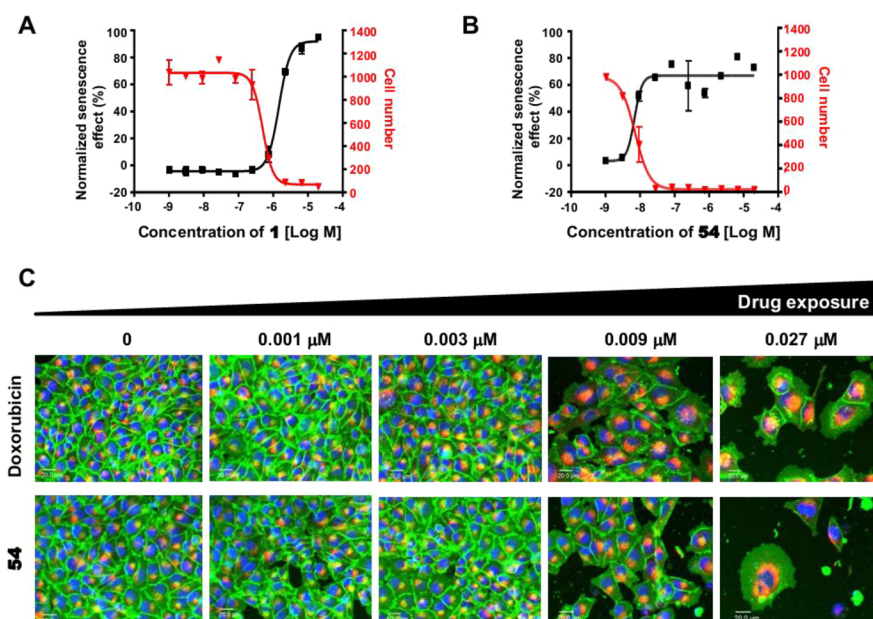


Figure 3. Identification of *N*-arylpiperidine-3-carboxamide derivatives to induce senescence-like phenotype in a dose-dependent manner. (A,B) Quantification of compounds **1** (A) or **54**-mediated cellular changes (B) in dose response. Human melanoma A375 cells were treated each compound in 3-fold dilution. After 3 days, cellular images were acquired using Opera and then analyzed by customized software. Red line means cell number, and black line means percentage of senescent cells per well. Z' value of assay validation was about 0.8. (C) Cellular images treated with doxorubicin and **54** in a dose-dependent manner. Scale bar is 20.0 μm . All experiments were duplicated.

conformations of compounds were processed with the LigPrep program,²⁹ and they were energy minimized with OPLS_2005 force field method. Next, the conformers were generated for each compound using a torsional search method with Confgen.³⁰ A total of 100 conformers per rotatable bonds were generated with the maximum number of conformers set as 1000 per compound. Phase program was used to generate the common pharmacophore hypothesis (CPH).³¹ The activity data of the compound were taken as negative logarithms of EC_{50} values. The activities of CPO compounds were classified as follows: (1) active compounds were considered as those with pEC_{50} values above -0.2 , and (2) inactive compounds were those with pEC_{50} values below -1.0 . Compounds were divided into both training and test sets based on structural diversity and coverage of the activity range. Pharmacophores from all conformations of compounds were examined, and all possible pharmacophore models having common features were identified. The minimum and maximum number of sites that a CPH may have was set to six. Also, it was set to match all tentative compounds. Among generated possible CPH, the best CPH was selected based on scoring. As the Phase program also provided the option to perform 3D-QSAR with the selected pharmacophore hypothesis, the atom-based QSAR model was built with default values for options.³¹

Out of twelve generated six featured hypotheses, the best CPH was selected as AHPRRR.11, based on having a higher survival score (survival score = 3.879) than others, as well as better predictive ability ($r^2 = 0.884$) from QSAR analysis. It was a six-point pharmacophore hypothesis with one hydrogen-bond acceptor (A), one hydrophobic group (H), one positively ionizable (P), and three aromatic rings (R) as pharmacophoric features. Active ligands were well-aligned with all six pharmacophoric features such as the most active compound **54** (Figure 4A): (1) Rings with substituents R^1 – R^3 are well-

represented by R11, R10, and R9 features, respectively; (2) the carbonyl group of the 3-carboxamide was represented by an A2 feature; and (3) *N*-piperidine was represented by both H7 and P8 features.

The best CPH clearly explained enantioselectivity for *N*-arylpiperidine-3-carboxamide of the compounds. The *S*-configuration **20** of the hit **1**, which was more active than that of racemic mixture **1**, was better mapped to the CPH than *R*-configuration **19**, which had a more than 15-fold increase than **20**. Due to angular difference between *S*- and *R*-configurations, the R11 feature was not mapped in the centroid of the A ring, 2,3-difluoro, in **19** (Figure 4E,F). Another notable mismapping was seen for the same R11 feature in **49**, where it is not flat but perpendicular to the planarity of R^1 group. Also, R9 and R10 features of **49** were out-of-plane against the rings in R^2 and R^3 groups. The A2 feature did not map with the carboxamide (Figure 4G). On the other hand, all pharmacophoric features mapped well with the active *S*-configuration **50** of racemate **48** (Figure 4H). These analyses clearly demonstrated structural differences of enantiomers significantly affected biological activity.

Additionally, a 3D-QSAR study was performed to establish relationship between the 3D pharmacophoric features and senescence-inducing activities. An atom-based QSAR was selected to better explain the SAR because it considered the entire molecular structure by treating a molecule as a set of overlapping van der Waals spheres.³² The 3D-QSAR results were visualized by a generated pictorial contours, with the blue cubes indicating favorable, while red cubes indicating unfavorable regions for activity (Figure 4B,D). Blue cubes surrounding amine in the linker indicated the inactivity of reverse-amide analogue (**17**) of the original scaffold. For R^3 substituents, blue cubes surrounding the 2-position of 2'-pyrrole suggested an increase in activity, whereas 3- and 5-positions were highlighted in the red cube, suggesting a

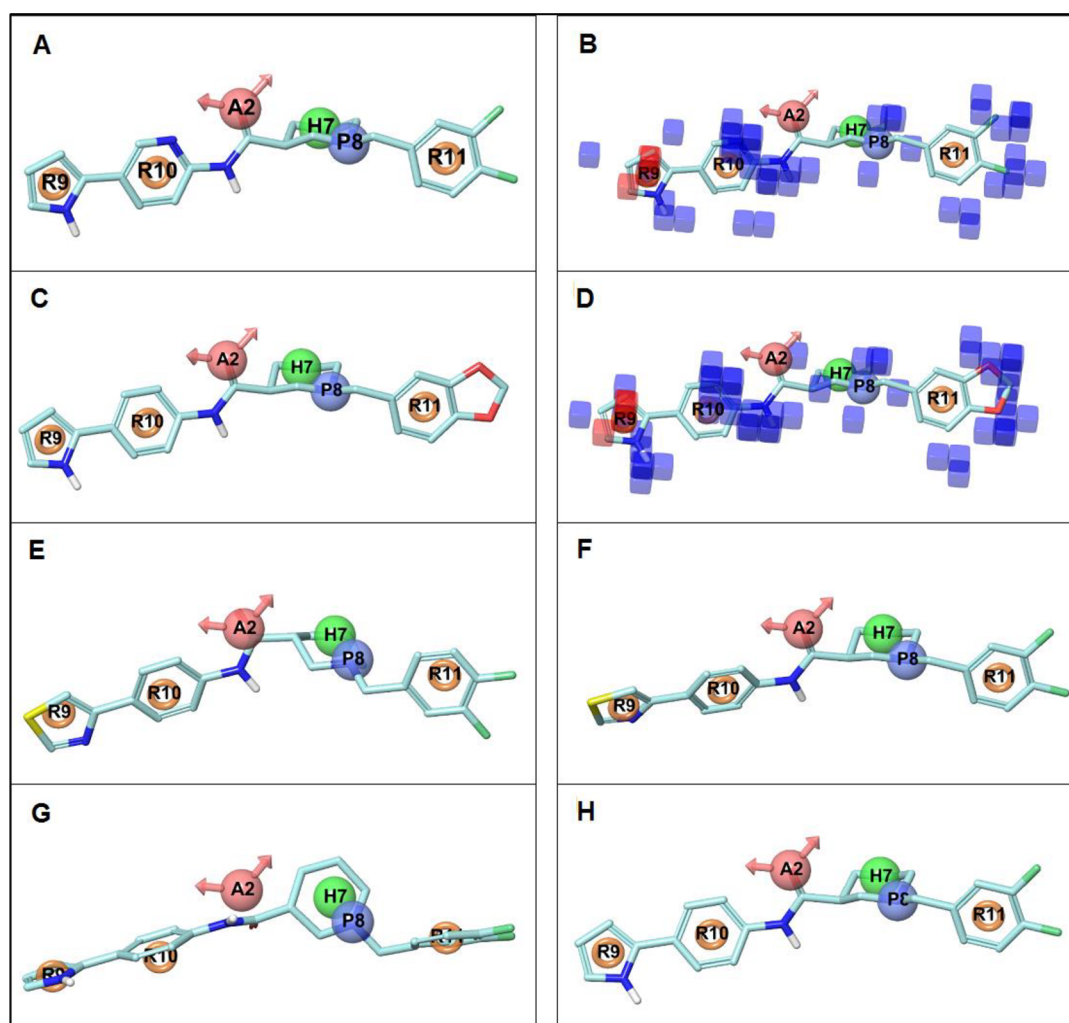


Figure 4. (A) Alignment of best fit compound **54** with the pharmacophore sites of the selected pharmacophore hypothesis, AHPRRR.11. Three aromatic ring features (R9, R10, and R11), one H-bond acceptor feature with lone pairs of electrons (A2), one positive ionizable (P8) feature, and one hydrophobic feature (H7) are shown in orange rings, pink spheres, a blue sphere, and a green sphere, respectively. (B) View of 3D-QSAR model with the most potent compound, **54**. The blue and red cubes show the structural features contributing positively and negatively to activity, respectively. (C) *S*-Configuration **51** is mapped well with CPH. (D) View of 3D-QSAR model with the active compound, **51**. (E) Less active *R*-configuration **19** is not mapped well with CPH. (F) *S*-Configuration **20** is mapped well with CPH. (G) Inactive *R*-configuration **49** is not aligned well with CPH. (H) Active *S*-configuration **50** is mapped well with CPH. All compounds are shown in atom-colored turquoise sticks.

decrease in activity such as with compounds **35** and **41**. The presence of electronegative atoms such as fluorine or oxygen, and their substitutional positions in R¹ in the A ring, had a strong influence on the senescent phenotype. A large number of blue cubes surrounded the 2,3,4-positions of the A ring and overlapped with the oxygen atoms of **51** (Figure 4D) as well as fluorine atoms of **54** (Figure 4B). The biological activity dramatically improved when benzene was replaced with pyridine in the B ring, and blue cubes were massed around the 1N atom in the B ring (Figure 4B). There was no cube representing the 2N atom in the B ring, which indicated a decrease in activity like that with compound **55**.

In order to understand structural requirements of molecules as melanoma senescence inducers, ligand-based pharmacophore model and atom-based 3D-QSAR studies were performed on a series of PCA derivatives to correlate their molecular architecture with senescence-inducing activity. The pharmacophore model well-explained the difference in biological activities between *S*- and *R*-configurations. Also, the detailed substituent in each group could be explained in

accordance with the activity. This derived model can provide guidance for the rational design of novel potent senescence inducers to treat melanoma.

As a cellular mechanism to avoid malignant transformation, cellular senescence has been considered a potential therapeutic target for cancer treatment.^{17,18,33} In order to discover a novel candidate for the treatment of melanoma, a newly developed whole-cell-based HTS and HCS assay was applied to pilot screen a small-molecule library containing ~110,000 diverse compounds, and a hit compound with *N*-arylpiperidine-3-carboxamide scaffold was discovered. To understand the structural aspects of the initial hit, 45 analogues with diverse modification in each moiety were designed and synthesized based on the original structure. Among them, **54**, a *S*-isomer with a pyridine ring in the B ring position, and pyrrole in R³, demonstrated improved antimelanoma activity (IC₅₀ = 0.03 μM) in accordance with markedly induced senescence-like morphological change (EC₅₀ = 0.04 μM) in human melanoma A375 cells. This compound also showed acceptable phase I metabolic stability. The novel series of *N*-arylpiperidine-3-

carboxamide derivatives proved the successful application of a newly developed HTS/HCS assay based on senescence-induced anticancer activities. Further studies including target identification and *in vivo* efficacy study are undergoing.

■ ASSOCIATED CONTENT

Supporting Information

The Supporting Information is available free of charge at <https://pubs.acs.org/doi/10.1021/acsmchemlett.0c00570>.

Supporting Tables SI-1 and SI-2 for cytotoxicity and phase I metabolic stability; experimental procedures for biological assays, synthetic procedures, and characterization data for presented compounds, including the spectral copies of ^1H and ^{13}C NMR spectra (PDF)

■ AUTHOR INFORMATION

Corresponding Authors

Myung Jin Kim – Functional Morphometry-I, Institut Pasteur Korea, Gyeonggi-do 13488, South Korea; Phone: +82-2-965-7977; Email: nanmolra1973@naver.com; Fax: +82-2-965-7976

Rita Song – Medicinal Chemistry Group, Institut Pasteur Korea, Gyeonggi-do 13488, South Korea; orcid.org/0000-0002-9992-7863; Phone: +82-2-577-1373; Email: rsong1228@gmail.com; Fax: +82-70-8677-1373

Authors

Sangmi Oh – Medicinal Chemistry Group, Institut Pasteur Korea, Gyeonggi-do 13488, South Korea; orcid.org/0000-0003-0895-1110

Do Yoon Kwon – Functional Morphometry-I, Institut Pasteur Korea, Gyeonggi-do 13488, South Korea

Inhee Choi – Medicinal Chemistry Group, Institut Pasteur Korea, Gyeonggi-do 13488, South Korea

Young Mi Kim – Medicinal Chemistry Group, Institut Pasteur Korea, Gyeonggi-do 13488, South Korea

Ji Young Lee – Functional Morphometry-I, Institut Pasteur Korea, Gyeonggi-do 13488, South Korea

Jiyoung Ryu – Medicinal Chemistry Group, Institut Pasteur Korea, Gyeonggi-do 13488, South Korea

Hangyeol Jeong – Functional Morphometry-I, Institut Pasteur Korea, Gyeonggi-do 13488, South Korea

Complete contact information is available at: <https://pubs.acs.org/doi/10.1021/acsmchemlett.0c00570>

Notes

The authors declare no competing financial interest.

■ ACKNOWLEDGMENTS

We are grateful to Dr. Shawn Yu in NIH/NIAID for his critical reading of this manuscript. This work was supported by the National Research foundation of Korea (NRF) grant funded by the Korea government (MSIP, Nos. 2007-00559 and 2010-002495, and MSIT, NRF-2017M3A9G6068257), Gyeonggi-do (No. K204EA000001-09E0100-00110), and KISTI.

■ REFERENCES

- (1) Kuilman, T.; Michaloglou, C.; Mooi, W. J.; Peeper, D. S. The essence of senescence. *Genes Dev.* **2010**, *24*, 2463–2479.
- (2) Rodier, F.; Campisi, J. Four faces of cellular senescence. *J. Cell Biol.* **2011**, *192*, 547–556.

- (3) Schmitt, C. A. Senescence, apoptosis and therapy—cutting the lifelines of cancer. *Nat. Rev. Cancer* **2003**, *3*, 286–295.

- (4) Bodnar, A. G.; Ouellette, M.; Frolkis, M.; Holt, S. E.; Chiu, C.-P.; Morin, G. B.; Harley, C. B.; Shay, J. W.; Lichtsteiner, S.; Wright, W. E. Extension of life-span by introduction of telomerase into normal human cells. *Science* **1998**, *279*, 349–352.

- (5) Ozturk, N.; Erdal, E.; Mumcuoglu, M.; Akcali, K. C.; Yalcin, O.; Senturk, S.; Arslan-Ergul, A.; Gur, B.; Yulug, I.; Cetin-Atalay, R.; et al. Reprogramming of replicative senescence in hepatocellular carcinoma-derived cells. *Proc. Natl. Acad. Sci. U. S. A.* **2006**, *103*, 2178–2183.

- (6) Gorbunova, V.; Seluanov, A.; Pereira-Smith, O. M. Expression of human telomerase (hTERT) does not prevent stress-induced senescence in normal human fibroblasts but protects the cells from stress-induced apoptosis and necrosis. *J. Biol. Chem.* **2002**, *277*, 38540–38549.

- (7) Chang, B. D.; Broude, E. V.; Dokmanovic, M.; Zhu, H.; Ruth, A.; Xuan, Y.; Kandel, E. S.; Lausch, E.; Christov, K.; Roninson, I. B. A senescence-like phenotype distinguishes tumor cells that undergo terminal proliferation arrest after exposure to anticancer agents. *Cancer Res.* **1999**, *59*, 3761–3767.

- (8) Ewald, J. A.; Desotelle, J. A.; Wilding, G.; Jarrard, D. F. Therapy-induced senescence in cancer. *J. Natl. Cancer Inst.* **2010**, *102*, 1536–1546.

- (9) Lee, S.; Lee, J.-S. Cellular senescence: a promising strategy for cancer therapy. *BMB Rep.* **2019**, *52*, 35–41.

- (10) Lee, S.; Schmitt, C. A. The dynamic nature of senescence in cancer. *Nat. Cell Biol.* **2019**, *21*, 94–101.

- (11) Yosef, R.; Pilpel, N.; Tokarsky-Amiel, R.; Biran, A.; Ovadya, Y.; Cohen, S.; Vadai, E.; Dassa, L.; Shahar, E.; Ben-Porath, I. Directed elimination of senescent cells by inhibition of BCL-W and BCL-XL. *Nat. Commun.* **2016**, *7*, 11190.

- (12) Zhu, Y.; Tchkonina, T.; Fuhrmann-Stroissnigg, H.; Dai, H. M. M.; Ling, Y. Y. Y.; Stout, M. B.; Pirtskhalava, T.; Giorgadze, N.; Johnson, K. O.; Giles, C. B.; Wren, J. D.; Niedernhofer, L. J.; Robbins, P. D.; Kirkland, J. L. Identification of a novel senolytic agent, navitoclax, targeting the Bcl-2 family of anti-apoptotic factors. *Aging Cell* **2016**, *15*, 428–435.

- (13) Tarunina, M.; Alger, L.; Chu, G.; Munger, K.; Gudkov, A.; Jat, P. S. Functional genetic screen for genes involved in senescence: role of Tid1, a homologue of the *Drosophila* tumor suppressor 1 (2) tid, in senescence and cell survival. *Mol. Cell. Biol.* **2004**, *24*, 10792–10801.

- (14) Bitler, B. G.; Fink, L. S.; Wei, Z.; Peterson, J. R.; Zhang, R. A high-content screening assay for small-molecule modulators of oncogene-induced senescence. *J. Biomol. Screening* **2013**, *18*, 1054–1061.

- (15) Lahtela, J.; Corson, L. B.; Hemmes, A.; Brauer, M. J.; Koopal, S.; Lee, J.; Hunsaker, T. L.; Jackson, P. K.; Verschuren, E. W. A high-content cellular senescence screen identifies candidate tumor suppressors, including EPHA3. *Cell Cycle* **2013**, *12*, 625–634.

- (16) Ewald, J. A.; Peters, N.; Desotelle, J. A.; Hoffmann, F. M.; Jarrard, D. F. A high-throughput method to identify novel senescence-inducing compounds. *J. Biomol. Screening* **2009**, *14*, 853–858.

- (17) Wang, B.; Kohli, J.; Demaria, M. Senescent Cells in Cancer Therapy: Friends or Foes? *Trends Cancer* **2020**, DOI: [10.1016/j.trecan.2020.05.004](https://doi.org/10.1016/j.trecan.2020.05.004).

- (18) Sherr, C. J.; Beach, D.; Shapiro, G. I. Targeting CDK4 and CDK6: From Discovery to Therapy. *Cancer Discovery* **2016**, *6* (4), 353–367.

- (19) Xue, W.; Zender, L.; Miething, C.; Dickins, R. A.; Hernandez, E.; Krizhanovskiy, V.; Cordon-Cardo, C.; Lowe, S. W. Senescence and tumour clearance is triggered by p53 restoration in murine liver carcinomas. *Nature* **2007**, *445*, 656–660.

- (20) Rakhra, K.; Bachireddy, P.; Zabuwala, T.; Zeiser, R.; Xu, L.; Kopelman, A.; Fan, A. C.; Yang, Q.; Braunstein, L.; Crosby, E.; et al. CD4+ T cells contribute to the remodeling of the microenvironment required for sustained tumor regression upon oncogene inactivation. *Cancer Cell* **2010**, *18*, 485–498.

- (21) Kang, T.-W.; Yeves, T.; Woller, N.; Hoenicke, L.; Wuestefeld, T.; Dauch, D.; Hohmeyer, A.; Gereke, M.; Rudalska, R.; Potapova, A.;

et al. Senescence surveillance of pre-malignant hepatocytes limits liver cancer development. *Nature* **2011**, *479*, 547–551.

(22) Oh, S.; Lee, J. Y.; Choi, I.; Ogier, A.; Kwon, D. Y.; Jeong, H.; Son, S. J.; Kim, Y.; Kwon, H.; Park, S.; Kang, H.; Kong, K.; Ahn, S.; Nehrbass, U.; Kim, M. J.; Song, R. Discovery of 4*H*-Chromeno[2,3-*d*]pyrimidin-4-one Derivatives as Senescence Inducers and Their Senescence-Associated Antiproliferative Activities on Cancer Cells using Advanced Phenotypic Assay. *Eur. J. Med. Chem.* **2021**, *209*, 112550.

(23) GENENTECH, Inc. Diazacarbazoles and methods of use. Patent Appl. WO/2009/151598, 2009.

(24) Germain, A. R.; Carmody, L. C.; Dockendorff, C.; Galan-Rodriguez, C.; Rodriguez, A.; Johnston, S.; Bittker, J. A.; MacPherson, L.; Dandapani, S.; Palmer, M.; et al. Identification of small-molecule inhibitors of *Trypanosoma cruzi* replication. *Bioorg. Med. Chem. Lett.* **2011**, *21*, 7197–7200.

(25) Sharma, D.; Narasimhan, B.; Kumar, P.; Judge, V.; Narang, R.; De Clercq, E.; Balzarini, J. Synthesis, antimicrobial and antiviral evaluation of substituted imidazole derivatives. *Eur. J. Med. Chem.* **2009**, *44*, 2347–2353.

(26) Yang, M.-Y.; Lin, P.-M.; Liu, Y.-C.; Hsiao, H.-H.; Yang, W.-C.; Hsu, J.-F.; Hsu, C.-M.; Lin, S.-F. Induction of cellular senescence by doxorubicin is associated with upregulated miR-375 and induction of autophagy in K562 cells. *PLoS One* **2012**, *7*, e37205.

(27) Bielak-Zmijewska, A.; Wnuk, M.; Przybylska, D.; Grabowska, W.; Lewinska, A.; Alster, O.; Korwek, Z.; Cmoch, A.; Myszk, A.; Pikula, S.; Mosieniak, G.; Sikora, E. A comparison of replicative senescence and doxorubicin-induced premature senescence of vascular smooth muscle cells isolated from human aorta. *Biogerontology* **2014**, *15*, 47–64.

(28) Sliwinska, M. A.; Mosieniak, G.; Wolanin, K.; Babik, A.; Piwocka, K.; Magalska, A.; Szczepanowska, J.; Fronk, J.; Sikora, E. Induction of senescence with doxorubicin leads to increased genomic instability of HCT116 cells. *Mech. Ageing Dev.* **2009**, *130*, 24–32.

(29) *LigPrep*, version 3.0; Schrödinger, LLC: New York, 2014.

(30) *ConfGen*, version 2.8; Schrödinger, LLC: New York, 2014.

(31) *Phase*, version 3.9; Schrödinger, LLC: New York, 2014.

(32) Shah, U. A.; Deokar, H. S.; Kadam, S. S.; Kulkarni, V. M. Pharmacophore generation and atom-based 3D-QSAR of novel 2-(4-methylsulfonylphenyl) pyrimidines as COX-2 inhibitors. *Mol. Diversity* **2010**, *14*, 559–568.

(33) Herranz, N.; Gil, J. Mechanisms and functions of cellular senescence. *J. Clin. Invest.* **2018**, *128*, 1238–1246.